nature structural & molecular biology

# Dual modes of RNA-silencing suppression by Flock House virus protein B2

Jeffrey A Chao[1,2], June Hyung Lee[1], Brian R Chapados[1], Erik W Debler[1], Anette Schneemann[1] & James R Williamson[1,2]

**As a counter-defense against antiviral RNA silencing during infection, the insect Flock House virus (FHV) expresses the silencing suppressor protein B2. Biochemical experiments show that B2 binds to double-stranded RNA (dsRNA) without regard to length and inhibits cleavage of dsRNA by Dicer *in vitro*. A cocrystal structure reveals that a B2 dimer forms a four-helix bundle that binds to one face of an A-form RNA duplex independently of sequence. These results suggest that B2 blocks both cleavage of the FHV genome by Dicer and incorporation of FHV small interfering RNAs into the RNA-induced silencing complex.**

© 2005 Nature Publishing Group http://www.nature.com/nsmb

FHV belongs to the Nodaviridae family of nonenveloped icosahedral viruses that have bipartite, positive-sense RNA genomes. RNA silencing, a conserved sequence-specific RNA regulatory pathway, acts as an antiviral defense mechanism in insects, the natural host of FHV[1]. After infection, the FHV genome and its replication intermediates can be processed by the RNase III enzyme, Dicer, into small interfering RNAs (siRNAs), which are 19–21 base pairs (bp) long with 5′-phosphates and 3′ 2-nucleotide (nt) overhangs. These FHV-derived siRNAs are then used to guide the RNA-induced silencing complex (RISC) to specifically degrade the viral genome. As a counter-defense mechanism, FHV encodes B2, a potent suppressor of RNA silencing[1]. B2 is a 106-residue protein that is synthesized at high levels early in the viral replication cycle; its mechanism of action is unknown[2]. FHV suppresses RNA silencing during replication in plant, insect and, as was recently shown, worm hosts, suggesting that B2 has evolved as a host-independent evasion mechanism[3–6].

Several plant viruses also encode RNA-silencing suppressors that use a variety of tactics to disrupt the silencing pathway[7]. Tombusvirus p19, the best characterized of these suppressors, binds to siRNAs corresponding to structured regions of the tombusvirus genome *in vivo*, thereby sequestering them from incorporation into the RISC[8,9]. The structure of p19 in complex with an siRNA shows that p19 binds along the length of the siRNA and positions a pair of tryptophan residues over the terminal base pairs[10,11]. Consequently, the length of the duplex in the siRNA is crucial for p19 recognition.

To define the RNA-silencing suppression mechanism of FHV B2, we undertook a biochemical and structural characterization of the interaction of B2 with dsRNA. B2 binds tightly ($K_d \sim 1$ nM) to dsRNA in a sequence-independent manner. RNA binding, unlike in p19, is not selective for siRNAs, as altering the length and termini (5′-phosphate and 3′ 2-nt overhang) did not disrupt binding. B2 also inhibited cleavage of a 35-bp RNA substrate by Dicer *in vitro*. A cocrystal structure of B2 in complex with an 18-bp dsRNA shows that B2 recognizes RNA as a dimer that forms a four-helix bundle. B2 interacts exclusively with the ribose-phosphate backbone of two successive minor grooves and the intervening major groove. Multiple B2 proteins can be modeled onto longer dsRNAs, suggesting that B2 may prevent Dicer processing by protectively coating the FHV genome. The ability to bind both long dsRNA and siRNAs allows B2 to suppress RNA silencing at two distinct steps of the silencing pathway.

## RESULTS

### Biochemical characterization of B2

Although there is no sequence homology between p19 and B2, it seemed plausible that B2 would also bind siRNAs because inhibition of RNA silencing at this level is host independent. The RNA binding of B2 to various short dsRNA constructs was quantitatively measured using a polyacrylamide gel electrophoretic mobility shift assay (EMSA). B2 binds specifically but sequence independently to dsRNA with high affinity (**Fig. 1a**) and does not recognize single-stranded RNA, double-stranded DNA or DNA-RNA hybrids (**Supplementary Fig. 1** online). In contrast to the binding specificity of p19, B2 RNA recognition is not specific for characteristic features of siRNAs. B2 binding affinity is not altered by the removal of the 5′-phosphate or 3′ 2-nt overhang, and B2 recognizes dsRNAs between 17 and 25 bp in length with comparable affinity (**Fig. 1b**). Duplexes shorter than 15 bp have >500-fold reduced binding affinity. B2 also binds to much longer dsRNAs (102 bp), though aggregation of the complex prevented quantitative measurement of the binding affinity (data not shown).

The distinct RNA-binding properties of B2 as compared to p19 suggest that B2 might function at a different stage of the RNA-silencing pathway. Addition of B2 to a Dicer *in vitro* cleavage assay

[1]Department of Molecular Biology and [2]Department of Chemistry and The Skaggs Institute for Chemical Biology, The Scripps Research Institute, 10550 N. Torrey Pines Rd., La Jolla, California 92037, USA. Correspondence should be addressed to J.W. (jrwill@scripps.edu).

Received 7 September; accepted 19 September; published online 9 October 2005; doi:10.1038/nsmb1005

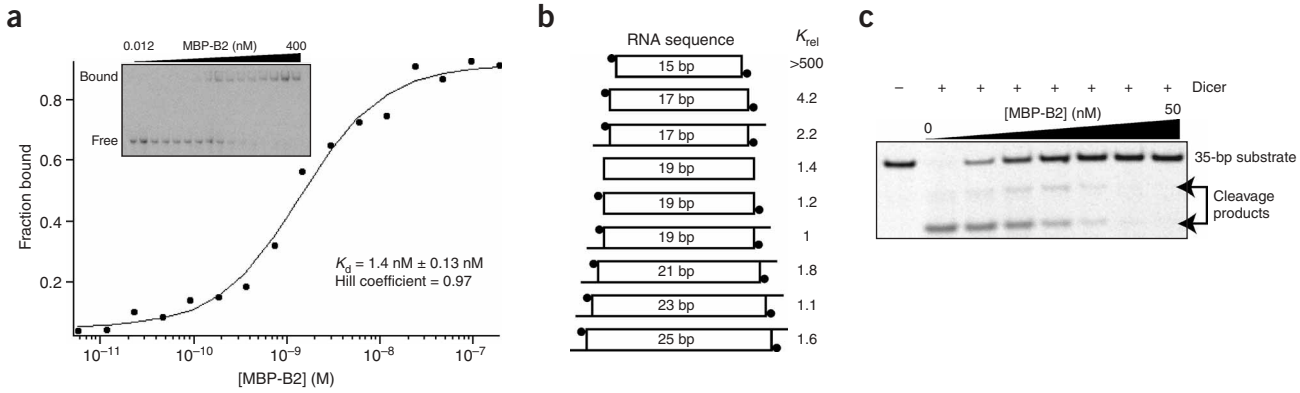


**Figure 1** Biochemical analysis of B2 dsRNA-binding specificity and Dicer inhibition. (**a**) Representative EMSA results from a 19-bp RNA duplex with 5′-phosphate and 3′ 2-nt overhang. A plot of the fraction of RNA bound as a function of MBP-B2 concentration is fit to the Hill equation, with raw data from gel image inset. Filled triangle represents MBP-B2 concentration increasing by a factor of 2 per lane from 0.012 nM to 400 nM. (**b**) Schematic of dsRNA constructs, comparing their relative binding affinities. $K_{rel}$ is the ratio of the $K_d$ to that of a 19-bp dsRNA with 5′-phosphate and 3′ 2-nt overhang. Circle, 5′-phosphate; extended line, 3′ 2-nt overhang. (**c**) Results of Dicer cleavage assay. A 35-bp dsRNA complex was incubated with Dicer and increasing concentration of MBP-B2. MBP-B2 efficiently inhibits cleavage of the substrate.

© 2005 Nature Publishing Group http://www.nature.com/nsmb

completely inhibits cleavage of a 35-bp dsRNA substrate (**Fig. 1c**). Similar results have been reported for other B2 and RNA constructs[3,6]. In contrast, p19 is ineffective in a similar assay[8]. Whereas B2 binding to dsRNA is not selective for siRNAs, B2 does bind to siRNAs with high affinity. Thus, it is also possible that B2 inhibits RNA silencing by preventing siRNA loading onto the RISC. B2 suppresses RNA silencing when siRNAs are used in *in vivo* assays, showing that B2 can function in silencing after Dicer cleavage as well[4,6,12]. B2 can apparently function both before and after Dicer processing, allowing B2 to act at two different points in the RNA-silencing pathway.

## Crystallization and structure determination

To define the mode of dsRNA recognition by B2, we crystallized a C-terminal truncation of B2 corresponding to residues 1–73 in complex with an 18-bp palindromic dsRNA. Full-length FHV B2 is not amenable to structural studies, necessitating the use of limited proteolysis and heteronuclear NMR to define the minimal functional construct. Initial truncations were identified by limited proteolysis with trypsin. A C-terminal truncation corresponding to residues 1–91 bound dsRNA with wild-type affinity (data not shown). Heteronuclear NMR experiments showed that residues at the C-terminus of this truncation were flexible and were not involved in RNA binding. Sequential assignment of the NMR resonances for this C-terminal region allowed the minimal construct to be identified with single–amino acid precision as residues 1–73. Although the C-terminal domain is dispensable for RNA binding, it may interact with other viral or host factors or mediate other functions during infection.

The $B2_{1–73}$–dsRNA complex was crystallized in both orthorhombic ($P2_12_12_1$) and tetragonal ($P4_122$) space groups. Both crystal forms contain one copy of the complex in the asymmetric unit and diffract to 2.6-Å resolution. The structure of the complex was solved by MAD on orthorhombic crystals that contained selenomethionine (SeMet)-labeled B2 (**Supplementary Fig. 2** online).

## Overview of B2–dsRNA complex

B2 binds dsRNA as a dimer and recognizes two adjacent minor grooves and the intervening major groove on one face of the RNA duplex (**Fig. 2a**). The intermolecular interface is formed by two symmetry-related α-helices and buries 1,757 Å$^2$ of combined solvent-accessible surface area (**Fig. 2b,c**). The long axis of the B2 dimer is rotated by ~10° in relation to the RNA helical axis, maximizing the interface with two successive minor grooves (**Fig. 2b**). The RNA helix is not substantially perturbed by protein binding and maintains A-form geometry, although the major groove is uniformly 2 Å wider and the minor groove is 1 Å narrower than in standard dsRNA.

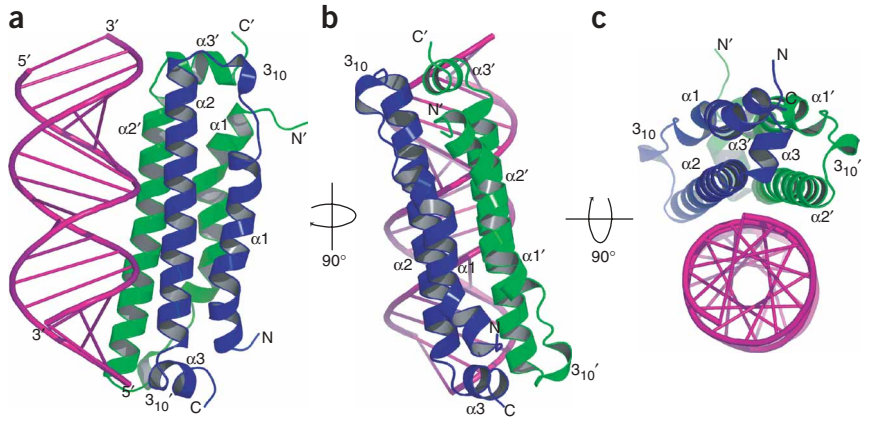


**Figure 2** Overall view of the B2–dsRNA complex. Blue and green, B2 dimer; magenta, RNA. N and C termini and secondary structure elements are labeled. (**a**) B2 binds dsRNA as a dimer and recognizes two successive minor grooves and the major groove that separates them. (**b**) The dimer is rotated by ~10° relative to the RNA to maximize contacts with both minor grooves. (**c**) The region of RNA that is bound by B2 dimers is localized to one face of the duplex. All figures were made using PyMOL (http://pymol.sourceforge.net).

### Structure of the B2 dimer

The B2 dimer forms a four-helix bundle by an antiparallel association of two B2 monomers that buries 2,394 Å$^2$ of combined solvent-accessible surface area. Each monomer is composed of three α-helices: the first two (α1 and α2) fold into a helix-turn-helix hairpin structure and the third, shorter α-helix (α3) packs perpendicular to the other two. A small $3_{10}$-helix stabilizes the extended loop that forms between α1 and α2. For clarity, a prime symbol denotes helices and residues located on the other protomer of the B2 dimer. In the dimer, helices α1 and α1′ and helices α2 and α2′ pack against each other, with α3 and α3′ located on opposite ends of the dimer (**Fig. 2a**,**b**). The B2 monomers are nearly identical (Cα r.m.s. deviation = 0.34 Å for 70 atoms), and because of the two-fold symmetry of the dimer, all of the interactions described for one monomer are also observed for its partner.

In the four-helix bundle formed by the B2 dimer, the monomers are almost collinear; in contrast, canonical left-handed antiparallel four-helix bundles have an interhelical angle of 20° (refs. 13,14). The B2 bundle is stabilized by a kink in α1 at Pro12 that allows hydrophobic residues located in α3 and in the loop and $3_{10}$-helix of the other B2 monomer to pack against the core of the dimer (**Supplementary Fig. 3** online). Notably, Pro12 is located at the 'a' position of heptad repeats found in canonical four-helix bundles, which is predicted to be highly unfavorable[15]. Algorithms for predicting secondary structure were unable to identify α1, which made it difficult to search for possible structural homology with known structures. Substitution of Pro12 with an alanine allows for the α-helices to be correctly predicted[16]. A structural similarity search of the Protein Data Bank using the DALI server did not identify any other four-helix bundles with similar architecture[17]. The proteins with the highest similarity (serine-tRNA ligase, 1SES, $Z$ = 6.4; vinculin, 1ST6, $Z$ = 6.0; topoisomerase I, 1A36, $Z$ = 6.0) form standard coiled-coil structures.

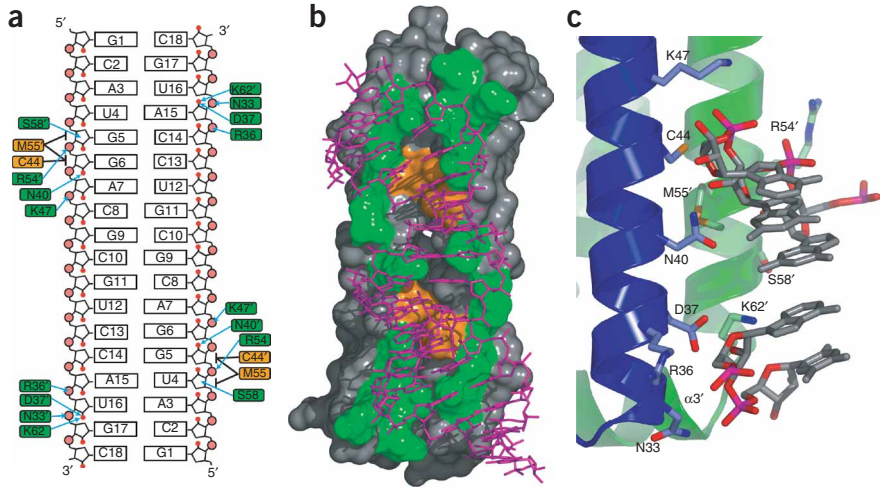


**Figure 3** Characterization of the RNA-protein interface of B2. (**a**) Schematic representation of RNA-protein interactions. Blue arrows, interactions with the phosphate backbone and sugars; black lines, van der Waals contacts. (**b**) Surface representation of the B2 dimer in complex with dsRNA. Green, residues that make polar contacts with the RNA; orange, van der Waals contacts. The positions of residues on the surface of the dimer allow for specific recognition of dsRNA. (**c**) Detailed view of the RNA-binding half-site. The RNA-binding domain of B2 is localized to α2 and α2′ and a majority of the interactions are with the minor groove. Stick side chains denote residues that contact the RNA.

### B2 shares structural similarity with Rop

Notably, the repressor of primer (Rop) protein from plasmid ColE1 that binds an RNA-kissing loop structure important for regulation of plasmid copy number also forms a four-helix bundle of similar size[18,19]. Several models of the Rop–RNA complex have been built on the basis of mutagenesis, NMR-shift mapping and mutational-envelope scanning[20–22]. If the kissing loop structure adopts a geometry close to A-form RNA, homology modeling with the B2 complex suggests that Rop could recognize a similar RNA binding site.

### RNA-protein interactions in the B2–dsRNA complex

The RNA-binding region of the B2 dimer is located primarily on the flat face of the molecule formed by α2 and α2′. In comparison, RNA recognition by Rop is mediated by the surface formed by α1 and α1′ (ref. 20). As predicted from the biochemical studies, the B2 RNA-binding interaction is sequence independent and is made up entirely of contacts with the phosphate backbone and ribose sugars (**Fig. 3a**). The locations of B2 residues that interact with the RNA duplex closely follow the position of the phosphate backbone (**Fig. 3b**). Lys47 and Arg54 of both α2 and α2′ contact the phosphate backbone in the major groove and divide the RNA-binding domain in half.

The majority of the RNA-protein interactions are clustered around the two minor grooves, which are recognized identically by the symmetric B2 dimer. At these locations, residues from both α2 and α2′ make several hydrogen bonds and electrostatic interactions with both strands of the dsRNA (**Fig. 3a**,**c**). After the major groove contacts made by Lys47 and Arg54′, the RNA-binding surface continues into one of the minor grooves, where Asn40 hydrogen bonds to the 2′-OH of the same ribose-phosphate backbone of the nucleotide recognized by Arg54′ (**Fig. 3c**). A van der Waals surface between Cys44 and Met55′ spans two adjacent ribose sugars, the second of which also contacts Ser58′. To bridge the minor groove, B2 contacts a dinucleotide step on the opposite RNA strand. Asn33, Arg36, Glu37 and Lys62′ interact with both the phosphates and a ribose 2′-OH of the dinucleotide step. The helix dipole of α3′ is positioned to interact with the phosphate backbone, completing the RNA-protein interface (**Fig. 3c**).

The van der Waals surface made by Cys44 and Met55′ is positioned in the center of the minor groove–recognition site (**Fig. 3b**). C44A and C44S mutants bind RNA with >100-fold reduced affinity, demonstrating an unusual role for cysteines in RNA-protein recognition (data not shown). An R54Q mutant has been reported to result in a 20-fold reduction in RNA binding[3], which is consistent with the electrostatic interaction made by Arg54 to a phosphate observed in the cocrystal structure.

The FHV and related Nodamura virus (NoV) B2 proteins share only marginal sequence similarity, yet probably adopt similar structures[23]. Almost all of the residues that contact the RNA are conserved between these proteins, as are Pro12 and many of the hydrophobic residues that form the core of the dimer. A noticeable exception is the variation of Cys44 and Met55, which make the van der Waals contact with the sugars in the minor groove. Perhaps these interactions are substituted by neighboring hydrophobic residues in NoV B2.

© 2005 Nature Publishing Group http://www.nature.com/nsmb

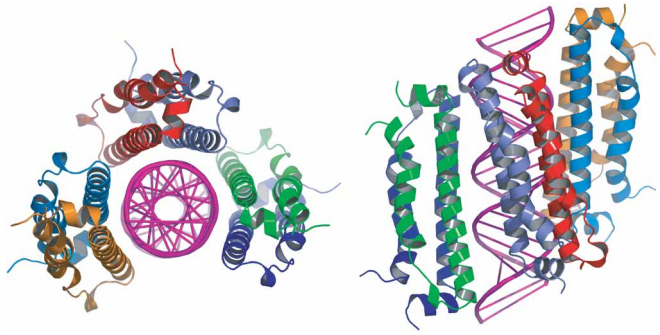

**Figure 4** Model of B2 bound to long dsRNA, in two orientations. A 24-bp dsRNA contains three complete B2-binding sites. Protective coating of dsRNA by B2 may inhibit Dicer processing.

## DISCUSSION

B2 and the canonical dsRNA-binding domain (dsRBD) represent distinct solutions to the problem of sequence-independent dsRNA recognition. The dsRBD adopts an αβββα fold that uses residues in both the α-helical and β-strand regions for RNA binding[24]. Both motifs recognize two minor grooves and the intervening major groove, but the recognition is performed by completely different protein architectures and backbone contacts. To investigate the specificity of the RNA-silencing pathway, dsRBDs from several proteins have been introduced into *in vivo* silencing assays and found to be effective suppressors[4,25].

Unlike these artificial systems, B2's sequence-independent recognition of dsRNA is vital to suppressing the antiviral RNA-silencing response of the host during FHV infection[1]. The mechanism of dsRNA recognition observed in the crystal structure is consistent with binding stoichiometry and ultracentrifugation experiments that indicate dsRNAs longer than 18 bp can bind multiple B2 dimers. A dsRNA 24 bp in length contains three complete B2 binding sites that can be occupied simultaneously by B2 dimers (**Fig. 4**). Such an arrangement could be extended along the surface of a much longer dsRNA to protectively coat it from Dicer processing. This model is consistent with recent studies of NoV B2 that show that the protein predominantly associates with Dicer precursor RNAs in the cell[6].

Biochemical studies and the general features of the structure suggest a dual role for B2 in suppressing RNA silencing by inhibiting both Dicer cleavage of viral RNA and the incorporation of cleaved viral RNAs into the RISC (**Fig. 5**). These two functions would provide an enormous benefit to the virus, which is subject to the constraints of a compact genome. Notably, NoV is also known to lethally infect mammals, raising the possibility that B2 may also function in inhibiting the PKR-interferon response, as in other animal viruses that encode dsRNA-binding proteins[26,27].

Recognition of dsRNA by the B2 four-helix bundle represents a new mode of RNA binding. The four-helix bundle is a common motif whose sequence space has been extensively mapped, yet it was not possible to predict the fold of B2 from its sequence. Cryptic four-helix bundles may exist in proteins implicated in RNA-binding that lack canonical motifs. The versatility of the four-helix bundle, as evidenced by this novel interaction, points to additional functions for these proteins in the rapidly expanding understanding of the role of dsRNA in the cell.

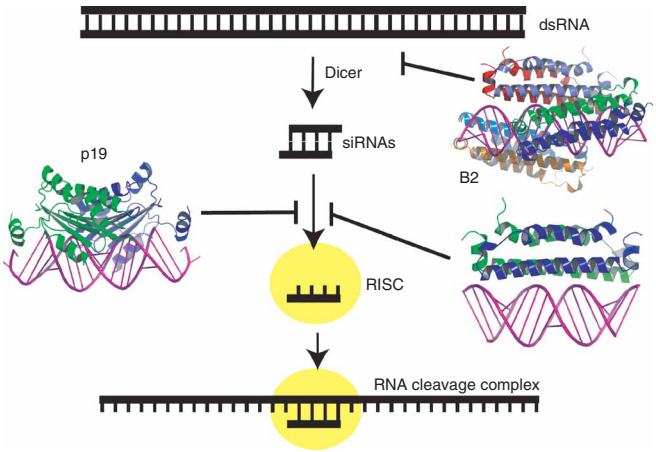


**Figure 5** Diagram of the RNA-silencing pathway. Suppression of certain stages of RNA silencing by B2 and p19 is indicated by solid lines. B2 can inhibit both Dicer cleavage and siRNA incorporation into RISC. p19 functions by preventing siRNA incorporation into RISC[10].

## METHODS

**Protein and RNA preparation.** Full-length B2 was cloned into pMalc (New England BioLabs) as an N-terminal maltose-binding fusion protein for use in biochemical studies. The fusion protein was expressed in *Escherichia coli* strain BL21(DE3). Recombinant protein was separated from nucleic acid by the addition of 0.1% (w/v) polyethyleneimine and purified by amylose affinity chromatography (New England BioLabs) followed by anion-exchange chromatography (Amersham Biosciences).

For structural studies, full-length FHV B2 was cloned into pET22HT, a variant of pET22b (Novagen) that contains an N-terminal $His_6$-tag and tobacco etch virus–protease cleavage site that replaces the pelB localization sequence. Limited trypsin proteolysis was used initially to determine that residues at the C terminus were more dynamic than the rest of B2. Heteronuclear NMR studies were used to define a minimal fragment corresponding to residues 1–73 and it was confirmed that the flexible C terminus was not involved in RNA binding. Truncations were prepared by PCR using the QuikChange site-directed mutagenesis kit (Stratagene). Native and SeMet-substituted B2 were expressed in *E. coli* strain BL21(DE3) and SeMet was incorporated by inhibition of methionine biosynthesis[28]. Recombinant protein was purified by nickel-chelating affinity chromatography (Qiagen) followed by anion-exchange chromatography (Amersham Biosciences). The $His_6$-tag was removed by TEV proteolysis (Invitrogen) and B2 was purified from the protease and uncleaved fusion protein by nickel-chelating affinity chromatography.

RNA constructs used for EMSAs and crystallization were prepared by chemical synthesis (Dharmacon) and deprotected, lyophilized and stored according to the manufacturer's protocol. RNAs used for crystallization were purified by denaturing PAGE. RNAs were annealed by incubation at 90 °C for 1 min followed by slow cooling to room temperature. The sequence of the palindromic RNA used for crystallization was 5′-GCAUGGACGCGUC CAUGC-3′, and the RNA sequences used for biochemical experiments are available upon request.

**Electrophoretic mobility shift assay.** The complex between MBP-B2 and RNA duplexes was monitored by EMSA experiments. 5′ end–labeled RNA constructs (20 pM) were equilibrated with a set of two-fold serial dilutions of MBP-B2 (~1 μM–12 pM). The complex was equilibrated in buffer containing 10 mM Tris (pH 7.5), 25 mM NaCl, 0.1 mM EDTA, 0.1 mg $ml^{-1}$ tRNA, 50 μg $ml^{-1}$ heparin and 0.01% (v/v) IGEPAL CA630 for at least 3 h. Protein–RNA complexes were resolved from unbound RNA by nondenaturing PAGE (4% (w/v) 29:1 acrylamide/bisacrylamide and 0.5× TBE) at 4 °C. Gels were dried and exposed to a PhosphorImager screen overnight (Molecular Dynamics). The fraction of bound RNA duplex was determined and fit to a modified version of the Hill equation as previously described[29].

© 2005 Nature Publishing Group http://www.nature.com/nsmb

**Table 1 Crystallographic data and structure refinement**

| | SeMet-B2$_{1-73}$–RNA | | | B2$_{1-73}$–5-BrU-RNA | |
|---|---|---|---|---|---|
| **Data collection** | | | | | |
| Space group | | $P2_12_12_1$ | | $P2_12_12_1$ | $P4_122$ |
| Cell dimensions | | | | | |
| *a*, *b*, *c* (Å) | | 51.5, 85.7, 92.3 | | 50.3, 86.2, 94.3 | 69.6, 69.6, 154.6 |
| α, β, γ (°) | | 90, 90, 90 | | 90, 90, 90 | 90, 90, 90 |
| | *Peak* | *Edge* | *Remote* | | |
| Wavelength (Å) | 0.9795 | 0.9797 | 0.9999 | 0.9190 | 0.9191 |
| Resolution (Å) | 84–4.2 | 84–4.2 | 84–3.0 | 34.4–2.55 | 35.6–2.60 |
| $R_{sym}$ | 0.117 (0.24)[a] | 0.112 (0.20) | 0.086 (0.46) | 0.123 (0.71) | 0.131 (0.61) |
| $I/\sigma I$ | 5.8 (3.4) | 6.3 (3.9) | 11.9 (2.7) | 10.0 (3.0) | 12.4 (5.1) |
| Completeness (%) | 97.5 (97.5) | 97.5 (97.5) | 97.9 (97.9) | 98.9 (98.9) | 100.0 (100.0) |
| Redundancy | 3.5 (3.7) | 3.5 (3.7) | 3.7 (3.9) | 6.7 (6.9) | 13.6 (13.5) |
| **Refinement** | | | | | |
| Resolution (Å) | | | | 34.4–2.6 | 35.6–2.6 |
| No. of reflections | | | | 13,054 | 12,323 |
| $R_{work}/R_{free}$ | | | | 24.9/26.7 | 24.5/26.4 |
| No. atoms | | | | | |
| Protein | | | | 1,083 | 1,074 |
| RNA | | | | 768 | 768 |
| Water | | | | 23 | 21 |
| *B*-factors | | | | | |
| Protein | | | | 41.2 | 41.3 |
| RNA | | | | 48.1 | 35.3 |
| Water | | | | 39.6 | 28.2 |
| R.m.s. deviations | | | | | |
| Bond lengths (Å) | | | | 0.007 | 0.006 |
| Bond angles (°) | | | | 1.17 | 1.15 |

[a]Values in parentheses indicate the high-resolution shells.

© 2005 Nature Publishing Group http://www.nature.com/nsmb

**Dicer cleavage assay.** A 5′ end–labeled 35-bp dsRNA substrate (0.1 nM) was added to Dicer cleavage buffer containing 20 mM Tris-HCl (pH 7.0), 150 mM NaCl, 2.5 mM magnesium acetate, 5 mM DTT, 5% (v/v) glycerol, 50 μg ml$^{-1}$ tRNA and 0.01% (v/v) Nonidet P-40. MBP-B2 was added in increasing concentrations and allowed to bind the RNA for 3 h at room temperature. Cleavage was then initiated by addition of 1 U Dicer (Stratagene) and the reactions incubated for 1 h at 37 °C. Cleavage products were extracted with phenol, resolved by electrophoresis through an 8% non-denaturing polyacrylamide gel (acrylamide/bisacrylamide = 19:1) and visualized by phosphorimaging.

**Crystallization and data collection.** The length of the RNA duplex was systematically varied during initial crystallization trials and a length of exactly 18 bp was found to be required for crystal formation. The dsRNA was mixed with B2 protein at a 2:1 protein/RNA ratio in 50 mM Tris (pH 7.5), 150 mM NaCl, 1 mM EDTA and 1 mM DTT. RNA–protein complexes were formed with native B2 and 5-bromouridine–substituted dsRNA as well as with SeMet-B2 and unlabeled dsRNA. Crystals were grown at 22 °C by hanging drop vapor diffusion by mixing equal volumes of complex and reservoir solution. Orthorhombic crystals ($P2_12_12_1$) of the SeMet-containing B2–RNA complex were grown from 10% (w/v) PEG 8,000, 50 mM sodium cacodylate (pH 6.5), 0.2 M KCl and 0.05 M magnesium acetate. The B2–bromouridine-RNA (B2–Br-RNA) complex crystallized in the same orthorhombic space group from 18% (w/v) PEG 3,350 and 0.2 M $MgSO_4$. In addition, a tetragonal crystal form ($P4_122$) was grown from 20% (w/v) MPEG 5,000, 0.2 M $(NH_4)SO_2$ and 0.15 M NaCl. Both crystal forms have one copy of the complex in the asymmetric unit. All crystals were transferred to mother liquor supplemented with 25% (v/v) glycerol before flash freezing in liquid nitrogen. A three-wavelength MAD data set was collected from the SeMet-B2–RNA complex on beamline 12.3.1 at the Advanced Light Source (**Table 1**). SAD data sets of the B2–Br-RNA complex were collected on beamline 11.1 at Stanford Synchrotron Radiation Laboratory. The diffraction data were processed using ELVES with MOSFLM and the CCP4 suite of programs[30–32].

**Structure determination.** Six selenium sites were located and initial phases were calculated using SOLVE and extended to 3.0 Å by maximum-likelihood density modification with RESOLVE (initial figure of merit = 0.46)[33]. After density modification (figure of merit = 0.54), the electron density maps were of sufficient quality to build a polyalanine trace of both B2 dimers and to locate the dsRNA[34]. SeMet side chains and other recognizable side chains were built appropriately. This model was then refined against both orthorhombic and tetragonal data sets collected from the B2–Br-RNA complex. Model building and refinement were performed using Xtalview and CNS[35,36]. Protein stereochemistry and RNA geometry were analyzed using PROCHECK and CURVES[37,38]. The final models of the B2 dimer contain residues 2–71 and 2′–72′ (orthorhombic) and residues 2–71 and 2′–71′ (tetragonal). Ramachandran analysis of both models shows that 100% of the backbone torsion angles are located in allowed regions.

**Accession codes.** Protein Data Bank: Coordinates have been deposited with accession codes 2AZ0 (orthorhombic) and 2AZ2 (tetragonal).

*Note: Supplementary information is available on the Nature Structural & Molecular Biology website.*

ACKNOWLEDGMENTS
This work was supported by the US National Institutes of Health (grants GM-53320 to J.R.W. and GM-53491 to A.S.), the Skaggs Institute for Chemical Biology and an Achievement Rewards for College Scientists Foundation fellowship to J.A.C. The authors wish to thank E. Sperling for assistance with protein

purification, M. Hennig for assistance with NMR spectroscopy and X. Dai, S. Nguyen, S. Ryder, R. Stanfield and R. Williams for helpful discussions.

COMPETING INTERSTS STATEMENT
The authors declare that they have no competing financial interests.

Published online at http://www.nature.com/nsmb/
Reprints and permissions information is available online at http://npg.nature.com/reprintsandpermissions/

1. Li, H., Li, W.X. & Ding, S.W. Induction and suppression of RNA silencing by an animal virus. *Science* **296**, 1319–1321 (2002).
2. Friesen, P.D. & Rueckert, R.R. Black beetle virus: messenger for protein B is subgenomic viral RNA. *J. Virol.* **42**, 986–995 (1982).
3. Lu, R. *et al.* Animal virus replication and RNAi-mediated antiviral silencing in *Caenorhabditis elegans*. *Nature* **436**, 1040–1043 (2005).
4. Li, W.X. *et al.* Interferon antagonist proteins of influenza and vaccinia viruses are suppressors of RNA silencing. *Proc. Natl. Acad. Sci. USA* **101**, 1350–1355 (2004).
5. Dasgupta, R., Garcia, B.H. II & Goodman, R.M. Systemic spread of an RNA insect virus in plants expressing plant viral movement protein genes. *Proc. Natl. Acad. Sci. USA* **98**, 4910–4915 (2001).
6. Sullivan, C.S. & Ganem, D. A virus-encoded inhibitor that blocks RNA interference in mammalian cells. *J. Virol.* **79**, 7371–7379 (2005).
7. Voinnet, O. Induction and suppression of RNA silencing: insights from viral infections. *Nat. Rev. Genet.* **6**, 206–220 (2005).
8. Lakatos, L., Szittya, G., Silhavy, D. & Burgyan, J. Molecular mechanism of RNA silencing suppression mediated by p19 protein of tombusviruses. *EMBO J.* **23**, 876–884 (2004).
9. Molnar, A. *et al.* Plant virus-derived small interfering RNAs originate predominantly from highly structured single-stranded viral RNAs. *J. Virol.* **79**, 7812–7818 (2005).
10. Vargason, J.M., Szittya, G., Burgyan, J. & Tanaka Hall, T.M. Size selective recognition of siRNA by an RNA silencing suppressor. *Cell* **115**, 799–811 (2003).
11. Ye, K., Malinina, L. & Patel, D.J. Recognition of small interfering RNA by a viral suppressor of RNA silencing. *Nature* **426**, 874–878 (2003).
12. Johnson, K.L., Price, B.D., Eckerle, L.D. & Ball, L.A. Nodamura virus nonstructural protein B2 can enhance viral RNA accumulation in both mammalian and insect cells. *J. Virol.* **78**, 6698–6704 (2004).
13. Crick, F.H.C. The packing of alpha-helices: simple coiled-coils. *Acta Crystallogr.* **6**, 689–697 (1953).
14. Harris, N.L., Presnell, S.R. & Cohen, F.E. Four helix bundle diversity in globular proteins. *J. Mol. Biol.* **236**, 1356–1368 (1994).
15. Lupas, A., Van Dyke, M. & Stock, J. Predicting coiled coils from protein sequences. *Science* **252**, 1162–1164 (1991).
16. Lupas, A. Prediction and analysis of coiled-coil structures. *Methods Enzymol.* **266**, 513–525 (1996).
17. Holm, L. & Sander, C. Dali/FSSP classification of three-dimensional protein folds. *Nucleic Acids Res.* **25**, 231–234 (1997).
18. Banner, D.W., Kokkinidis, M. & Tsernoglou, D. Structure of the ColE1 rop protein at 1.7 A resolution. *J. Mol. Biol.* **196**, 657–675 (1987).
19. Tomizawa, J. & Som, T. Control of ColE1 plasmid replication: enhancement of binding of RNA I to the primer transcript by the Rom protein. *Cell* **38**, 871–878 (1984).
20. Predki, P.F., Nayak, L.M., Gottlieb, M.B. & Regan, L. Dissecting RNA-protein interactions: RNA-RNA recognition by Rop. *Cell* **80**, 41–50 (1995).
21. Comolli, L.R., Pelton, J.G. & Tinoco, I., Jr. Mapping of a protein-RNA kissing hairpin interface: Rom and Tar-Tar*. *Nucleic Acids Res.* **26**, 4688–4695 (1998).
22. Christ, D. & Winter, G. Identification of functional similarities between proteins using directed evolution. *Proc. Natl. Acad. Sci. USA* **100**, 13202–13206 (2003).
23. Johnson, K.N., Johnson, K.L., Dasgupta, R., Gratsch, T. & Ball, L.A. Comparisons among the larger genome segments of six nodaviruses and their encoded RNA replicases. *J. Gen. Virol.* **82**, 1855–1866 (2001).
24. Ryter, J.M. & Schultz, S.C. Molecular basis of double-stranded RNA-protein interactions: structure of a dsRNA-binding domain complexed with dsRNA. *EMBO J.* **17**, 7505–7513 (1998).
25. Lichner, Z., Silhavy, D. & Burgyan, J. Double-stranded RNA-binding proteins could suppress RNA interference-mediated antiviral defences. *J. Gen. Virol.* **84**, 975–980 (2003).
26. Brandt, T.A. & Jacobs, B.L. Both carboxy- and amino-terminal domains of the vaccinia virus interferon resistance gene, E3L, are required for pathogenesis in a mouse model. *J. Virol.* **75**, 850–856 (2001).
27. Chien, C.Y. *et al.* Biophysical characterization of the complex between double-stranded RNA and the N-terminal domain of the NS1 protein from influenza A virus: evidence for a novel RNA-binding mode. *Biochemistry* **43**, 1950–1962 (2004).
28. Doublie, S. Preparation of selenomethionyl proteins for phase determination. *Methods Enzymol.* **276**, 523–530 (1997).
29. Recht, M.I. & Williamson, J.R. Central domain assembly: thermodynamics and kinetics of S6 and S18 binding to an S15-RNA complex. *J. Mol. Biol.* **313**, 35–48 (2001).
30. Leslie, A.G.W. Recent changes to the MOSFLM package for processing film and image plate data. *Joint CCP4 + ESF-EAMCB Newsletter on Protein Crystallography* No. 26 (1992).
31. Holton, J. & Alber, T. Automated protein crystal structure determination using ELVES. *Proc. Natl. Acad. Sci. USA* **101**, 1537–1542 (2004).
32. Collaborative Computational Project Number 4. The CCP4 suite: programs for protein crystallography. *Acta Crystallogr. D Biol. Crystallogr.* **50**, 760–763 (1994).
33. Terwilliger, T.C. & Berendzen, J. Automated MAD and MIR structure solution. *Acta Crystallogr. D Biol. Crystallogr.* **55**, 849–861 (1999).
34. Terwilliger, T. Maximum likelihood density modification. *Acta Crystallogr. D Biol. Crystallogr.* **56**, 965–972 (2000).
35. Brunger, A.T. *et al.* Crystallography & NMR system: a new software suite for macromolecular structure determination. *Acta Crystallogr. D Biol. Crystallogr.* **54**, 905–921 (1998).
36. McRee, D.E. XtalView/Xfit—A versatile program for manipulating atomic coordinates and electron density. *J. Struct. Biol.* **125**, 156–165 (1999).
37. Lavery, R. & Sklenar, H. The definition of generalized helicoidal parameters and of axis curvature for irregular nucleic acids. *J. Biomol. Struct. Dyn.* **6**, 63–91 (1988).
38. Laskowski, R.A., MacArthur, M.W., Moss, D.S. & Thornton, J.M. PROCHECK: a program to check the stereochemical quality of protein structures. *J. Appl. Crystallogr.* **26**, 283–291 (1993).

© 2005 Nature Publishing Group http://www.nature.com/nsmb